frontiers | Frontiers in Earth Science

TYPE Original Research
PUBLISHED 27 January 2023
DOI 10.3389/feart.2023.1122109

OPEN ACCESS

EDITED BY
Zhenzhi Wang,
Henan Polytechnic University, China

REVIEWED BY
Decheng Zhang,
Hebei University of Technology, China
Qiang Chen,
Chongqing University, China
Jun Liu,
Sichuan University, China

*CORRESPONDENCE
Run Chen,
chenrun@cumt.edu.cn

SPECIALTY SECTION
This article was submitted to Economic Geology, a section of the journal Frontiers in Earth Science

RECEIVED 12 December 2022
ACCEPTED 13 January 2023
PUBLISHED 27 January 2023

CITATION
Chen R, Hu K, Lv F and Zhang Y (2023), Effect of supercritical CO_2 extraction on pore characteristics of coal and its mechanism.
Front. Earth Sci. 11:1122109.
doi: 10.3389/feart.2023.1122109

Effect of supercritical CO_2 extraction on pore characteristics of coal and its mechanism

Run Chen[1,2]*, Kunpeng Hu[1,2], Fengrong Lv[1,2] and Yajun Zhang[1,2]

[1]Jiangsu Key Laboratory of Coal-based Greenhouse Gas Control and Utilization (Carbon Neutrality Institute), China University of Mining and Technology, Xuzhou, China, [2]School of Resources and Geosciences, China University of Mining and Technology, Xuzhou, China

Abundant pore space in coal is not only the place for the accumulation of coalbed methane (CBM), but also the tunnel for gas migration. In this study, five sets of coal samples before and after the second coalification were selected from the eastern margin of Ordos Basin to simulate supercritical CO_2 (Sc-CO_2) extraction in supercritical extraction equipment. The evolutions of pore structure and porosity were tested by mercury intrusion porosimetry and nuclear magnetic resonance spectroscopy to compare the changes of pore structure and porosity due to the Sc-CO_2 extraction, and to explain the related mechanism. The results show that: (1) Pore volume, pore specific surface area, and connectivity characteristics changed significantly due to Sc-CO_2 extraction, and the increment of pore volume and pore specific surface area presented a law of increase–decrease–increase with the increase in the coal rank, and the turning point was near the second coalification. (2) The porosity increment change trend due to Sc-CO_2 extraction was increase–decrease–increase with increasing coal rank, and the turning point was again near the second coalification, which supports the mercury intrusion porosimetry results. (3) The changes were observed in the porosity characteristics due to Sc-CO_2 extraction through pore-increasing and expanding effects. Before the second coalification, the pore-increasing and expanding effects co-existed in the micropores, and after the second coalification, the pore-expanding effect mainly existed in the transitional pores and above. (4) The variation model for the pore structure of coal due to Sc-CO_2 extraction was established. The conclusions offer not only important theoretical significance for the CO_2-enhanced CBM (CO_2-ECBM) mechanism but also important significance for CO_2-ECBM engineering.

KEYWORDS

SC-CO2 extraction, pore structure, porosity, mechanism, coal rank

1 Introduction

Coal is a heterogeneous porous medium, in which the structure is characterized as a dual pore system that includes original porosity and secondary porosity (Wang et al., 2018). The original porosity includes microspores, transitional pores, and mesopores in the coal matrix, the gas adsorbs/desorbs on/from the coal matrix, and undergoes diffusion. The secondary porosity is composed of non-uniformly distributed macropores and microfractures, and gas diffuses and seeps in it (Fu et al., 2005; Chen et al., 2021; Liu et al., 2022; Xu and Qin, 2022).

In recent decades, extensive research efforts have been devoted to the study of the pore structure of coal for systematic exploration of the causes and influencing factors of pore structure. The pores were found to be formed during the process of coalification (Wang and Chen, 1995; Zhang, 2001; Wu et al., 2016). Tang et al. (2008) found that the porosity, pore structure, and specific surface area of coal were controlled by the degree of coal metamorphism

based on the results of mercury intrusion porosimetry and nitrogen adsorption test. Liu Y. W. et al. (2020) found that the Brunauer–Emmett–Teller (BET) specific surface area of coal increased and then decreased with the increase of coal rank, the micropores decreased and then increased, and the small pores and mesopores increased, and then decreased as indicated by low-temperature nitrogen adsorption test. Yang et al. (2021) found that the proportion of micropores and small pores gradually increased and that of mesopores and macropores gradually decreased with the increase of coal rank by low-field nuclear magnetic resonance (NMR) spectroscopy test. Zhao et al. (2010) found that the coal porosity, micropore volume, and BET surface area of coal showed high–low–high variation pattern with the increase of coal rank through vitrinite reflectance test, mercury intrusion porosimetry, and low-temperature nitrogen adsorption test. Liu H. F. et al. (2020) studied the surface pore morphology of coal by scanning electron microscopy (SEM) and found that the surface porosity of coal samples increased with the increase in the degree of coalification. Zhu et al. (2019) studied the pore characteristics of coal by NMR spectroscopy and found that the total porosity first decreased and then increased with the increase of coal rank. Moreover, it has been found that the pore structure of coal is affected by many geological factors and their coupling, such as mineral content, maceral composition, coal structure type, and tectonic stress (Lv et al., 1991; Fu et al., 2007; Du et al., 2018).

Notably, some techniques and approaches are available to change the pore structure of coal. For example, injecting CO_2 into coal reservoirs can dissolve carbon rock salt minerals present in coal, destroy the macromolecular structure, and extract functional groups, which leads to an increase in the specific surface area, total pore volume, and porosity of coal (Guo et al., 2018; Zhang et al., 2019; Zhang et al., 2020; Wang et al., 2021). Moreover, Yuan et al. (2022) found that the pore structure of coal samples changed after the freeze-thaw cycle, and the number of large pores and medium pores increased. Di et al. (2022) found that microbial participation in coal reservoir degradation could stabilize pore size, make pores smoother, reduce specific surface area, and increase pore volume. Si et al. (2021) observed that the intrusion of water reduced the type and content of minerals in coal, resulting in an increase in pore volume.

The above-mentioned studies indicate that the characteristics of the pore structure of coal and its influencing factors have been extensively explored. However, supercritical (Sc)-CO_2 that offers a better ability to transform the pore structure of coal, resulting in significant changes in pore structure, has not been extensively investigated to date. Notably, Sc-CO_2 can extract small organic molecules from the coal matrix, change the pore structure characteristics of coal, and affect the recovery and storage effect of CO_2-enhanced coal bed recovery (CO_2-ECBM) (Wang, 2018; Zhang, 2019; Sampath et al., 2020; Wang et al., 2022). In this study, five sets of coal samples before and after the second coalification ($R_{o,max}$ = 1.3%) were selected from the eastern margin of Ordos Basin to simulate the process of Sc-CO_2 extraction of small organic molecules from coal under geological conditions. The mercury intrusion porosimetry and NMR spectroscopy were used to analyze the transformation of coal pore structure and porosity by Sc-CO_2 extraction, and the evolving relationship with coal rank was discussed. The mechanism was revealed and the geological model was constructed, in order to provide a basis for theoretical research and engineering implementation of replacement CBM extraction and CO_2-ECBM.

2 Experimental

2.1 Collection of coal samples

The Ordos basin is a large stable craton basin, which is rich in fossil energy. The geological structure of the basin is relatively simple. It is distributed in a north-south direction, showing the structural characteristics of north-south zonation and east-west zonation, and has experienced the evolution of a multi-stage tectonic cycle (Zhang, 2019).

The main coal-bearing strata are the Upper Carboniferous-Lower Permian Taiyuan Formation and Lower Permian Shanxi Formation. The formations of Benxi, Taiyuan, Shanxi, Lower Shihezi, Upper Shihezi, and Shiqianfeng are the main coal-bearing formations, which consist principally of coal, limestone, siltstone, and sandstone (Chen et al., 2017). Hedong coalfield is one of the six major coalfields in Shanxi Province and is a typical Carboniferous-Permian coalfield. There are 6–15 layers of coal, among which 6 to 8 layers can be mined, with an average thickness of 7–28 m. The coal rank gradually increases from north to south.

In order to investigate the influence of coal rank on Sc-CO_2 extraction and avoid the influence of geological structure, five undeformed coal samples distributed around the second coalification were collected from the Hedong Coalfield of the eastern edge of the Ordos Basin (Figure 1). The physical properties of the coals investigated in this study are listed in Table 1. The maximum vitrinite reflectance under oil immersion ($R_{o,max}$) of the coals varies from 0.76% to 2.01%. The proximate analysis result shows that the equilibrated moisture varies from 0.18% to 1.54%, the ash yield varies from 6.70% to 21.07%, and the volatile matter varies from 14.29% to 29.49% for the five coal samples. The ultimate analysis result shows that the carbon content varies from 82.50% to 89.36%, the hydrogen content varies from 4.21% to 4.81%, and the oxygen content varies from 1.74% to 10.96% for the five coal samples.

To avoid oxidation during the transportation of specimens and also during the time required to carry out Sc-CO_2 extraction, the coal samples were stored *via* vacuum packaging and sealed in plastic bags. A cylinder with dimensions of 25 mm × 25 mm was prepared in the laboratory for the NMR test and the square coal block with a side length of 1.5 cm was used for the mercury intrusion porosimetry. The prepared coal samples were divided into two parts, one for Sc-CO_2 extraction experiments and the other for comparative analysis. In order to reduce the mineralization reaction between CO_2 in the water environment and minerals in the coal matrix, the necessary drying treatment of the coal pillar was carried out before the experiment.

2.2 Experimental methods

2.2.1 Sc-CO_2 extraction experiment

A high-temperature and pressure reaction kettle (TC-2, Jiangsu Tuochuang Scientific Instrument Limited Liability Company, Nantong, China) was used as the experimental equipment. The experimental temperature was adjusted to ~45°C, the pressure was adjusted to ~10 MPa, and the extraction time was 96 h. The flow chart

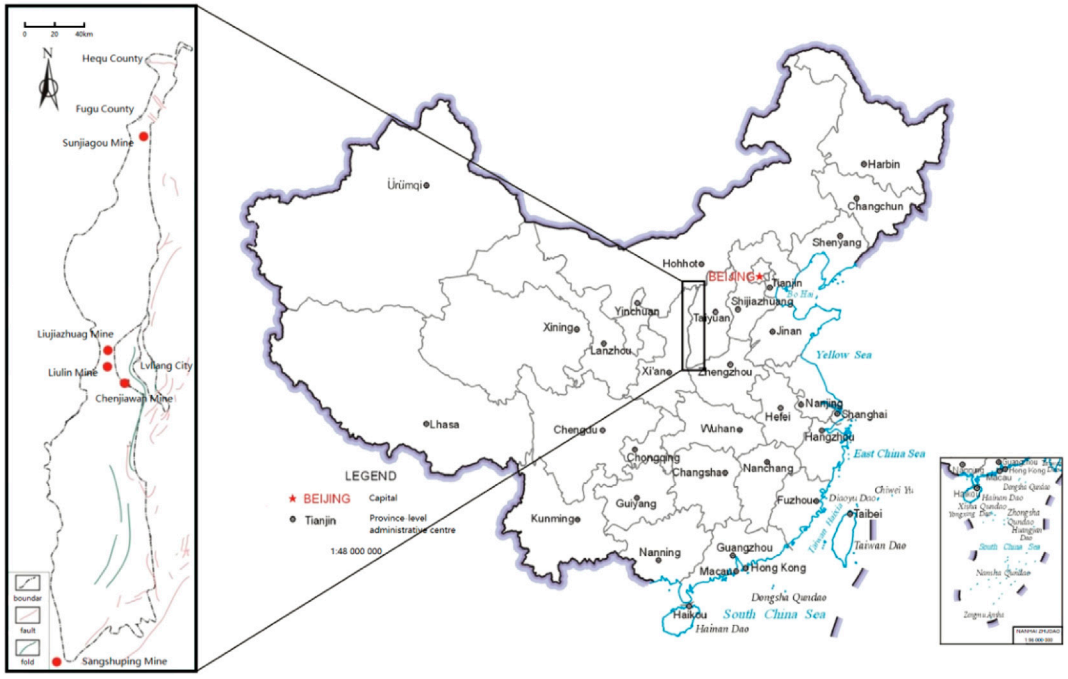

FIGURE 1
Location of coal samples collected.

TABLE 1 The results of $R_{o,max}$ proximate analysis and ultimate analysis.

Sample	$R_{o,max}$	Proximate analysis (%)				Ultimate analysis (%)				
		M_{ad}	A_d	V_{daf}	FC_d	$S_{t,d}$	C_{daf}	H_{daf}	O_{daf}	N_{daf}
SJG coal	0.76	1.54	11.05	29.49	62.72	0.63	82.50	4.41	10.96	1.43
LJZ coal	1.00	0.94	17.56	26.85	60.31	0.38	85.42	4.81	7.86	1.44
LL coal	1.20	0.77	21.07	19.88	63.24	0.52	86.53	4.21	7.32	1.28
CJW coal	1.56	0.45	6.70	18.94	75.63	1.07	89.36	4.46	3.48	1.55
SSP coal	2.01	0.18	9.60	14.29	77.48	5.79	86.66	4.23	1.74	0.96

of Sc-CO_2 extraction is shown in Figure 2. The operating steps are as follows.

1) The extraction cell was opened and the coal pillar was placed in the supercritical extraction cell, which was then covered with a cauldron and the screws were tightened to ensure a good seal.
2) The CO_2 gas cylinder valve was opened to allow the CO_2 gas to flow through the purifier and the cooling system, after which it was eventually compressed into the extraction cell. After the pressure and temperature of the cell were adjusted to ~10 MPa and 45°C, respectively, the CO_2 gas cylinder valve was closed to ensure that the extraction cell remained under the designed condition. The temperature and pressure were monitored throughout the process.
3) After 96 h of Sc-CO_2 extraction, the supercritical equipment was shut down, the gas was released to bring the pressure of the extraction cell to the atmospheric pressure, and the coal sample was collected after the extraction cell was cooled down to room temperature, the separation cells were washed with a solvent, and the waste liquid was collected for testing.

2.2.2 Mercury intrusion porosimetry

In this study, pore size distribution, surface area, and pore connectivity were investigated by mercury intrusion porosimetry (AutoPore IV9500, Micromeritics Instrument Crop, Norss, GA, United States). Mercury intrusion porosimetry is based on the capillary flow governing liquid penetration in small pores. This law, in the case of a non-wetting liquid such as mercury, is expressed by using the Washburn equation (Washburn, 1921):

$$D = \left(\frac{1}{P}\right)4\gamma \cos\varphi \quad (1)$$

where D is the diameter of the pore, P is the applied pressure, γ is the surface tension of mercury, and φ is the contact angle between the mercury and the sample, all in consistent units. In this study, the

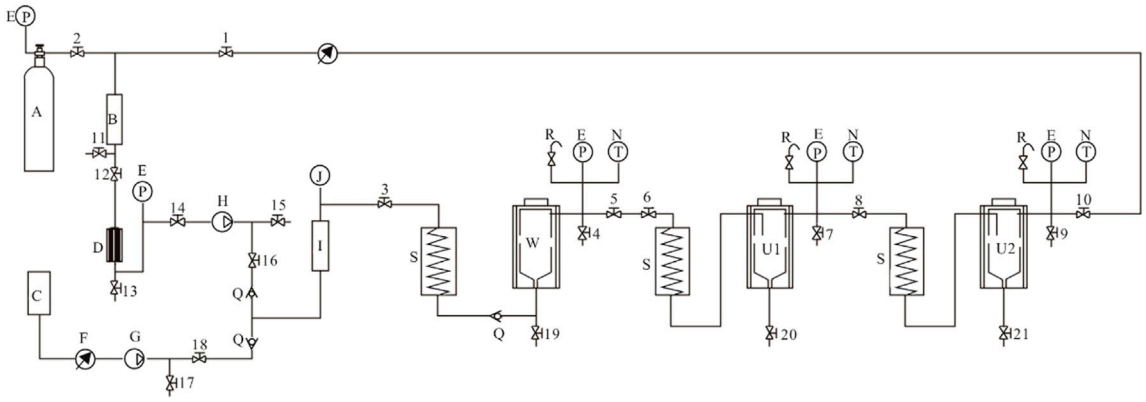

FIGURE 2
The flow chart of SC-CO_2 extraction experiment. **(A)** CO_2 cylinder; **(B)** Purifier; **(C)** Carry dose bucket; **(D)** Cold condenser; **(E)** Pressure gauge; **(F)** Carrier flowmeter; **(G)** Carrier pump; **(H)** High pressure CO_2 pump; **(I)** Mixer; **(J)** Electric contact pressure gauge; **(N)** Thermometer; **(P)** CO_2 flowmeter; **(Q)** Check valve; **(R)** Safety valve; **(S)** Pre-heater; U1: Separation kettle; **(W)** Extraction kettle; 1–5, 7–21: Stop valve; 6: Regulating valve.

TABLE 2 Pore volumes of the samples before and after the Sc-CO_2 extraction.

Coal sample		Volume ($cm^3 \cdot g^{-1}$)					Proportion (%)			
		V_{mi}	V_{tr}	V_{me}	V_{ma}	V_t	V_{mi}/V_t	V_{tr}/V_t	V_{mei}/V_t	V_{ma}/V_t
SJG	Raw coal	0.0115	0.0211	0.0026	0.0041	0.0395	29.26	53.58	6.69	10.47
	Sc-CO_2 extracted coal	0.0145	0.0173	0.0030	0.0054	0.0401	36.09	43.11	7.40	13.40
LJZ	Raw coal	0.0042	0.0055	0.0009	0.0025	0.0132	32.16	41.86	6.78	19.20
	Sc-CO_2 extracted coal	0.0053	0.0070	0.0024	0.0065	0.0211	24.90	33.00	11.14	30.96
LL	Raw coal	0.0028	0.0032	0.0010	0.0025	0.0096	29.47	33.24	10.79	26.50
	Sc-CO_2 extracted coal	0.0038	0.0048	0.0010	0.0018	0.0114	32.96	42.23	8.86	15.95
CJW	Raw coal	0.0060	0.0075	0.0016	0.0064	0.0216	27.85	34.91	7.57	29.66
	Sc-CO_2 extracted coal	0.0066	0.0083	0.0036	0.0087	0.0273	24.17	30.53	13.25	32.05
SSP	Raw coal	0.0064	0.0079	0.0021	0.0070	0.0234	27.16	33.80	9.03	30.01
	Sc-CO_2 extracted coal	0.0069	0.0089	0.0021	0.0123	0.0303	22.87	29.29	7.03	40.82

V_{mi}: Micropore volume; V_{tr}: Transitional pore volume; V_{me}: Mesopore volume; V_{ma}: Macropore volume; V_t: Total pore volume.

surface tension was 485 $dyn \cdot cm^{-1}$, the contact angle between the mercury and coal sample was 130°, and the density of mercury was 13.5335 $g \cdot mL^{-1}$.

2.2.3 Nuclear magnetic resonance test

In this study, porosity was investigated using a cabinet NMR low-temperature porosity analyzer (NMRC12-010V, Suzhou Niumag analytical instrument Limited Liability Company, Suzhou, China). Notably, the NMR signal is proportional to the water content of the sample for the same test parameters (Zheng et al., 2018). The pores of the sample were filled with water, and a set of standard samples with known water content was first tested to fit with a curve of water content and NMR signal volume. Then, the measured NMR signal volume of the sample was substituted into the curve equation to find the water content in the sample. Pore volume was calculated according to moisture content and porosity was derived by combining sample volume (Liu et al., 2019; Zheng et al., 2019; Xiong et al., 2022; Zhao et al., 2022).

The NMR experiments were performed using 25 mm coils, the experimental temperature was 32°C, and the resonance frequency was 12 MHz. Besides, in the NMR test, the sample signal was collected according to the Carr–Purcell–Meiboom–Gill (CPMG) sequence, echo spacing (T_E) was 0.35 m, waiting time (T_W) was 6000 m, echo number (NECH) was 4096, and scan time (N_S) was doubled.

3 Results and discussion

In this study, the Чодот В. В. (Чодот, 1966). decimal classification method was used to classify the pore structure types in coal. That is micropore (<10 nm), transitional pore (10–100 nm), mesopore (100–1000 nm), and macropore (>1000 nm).

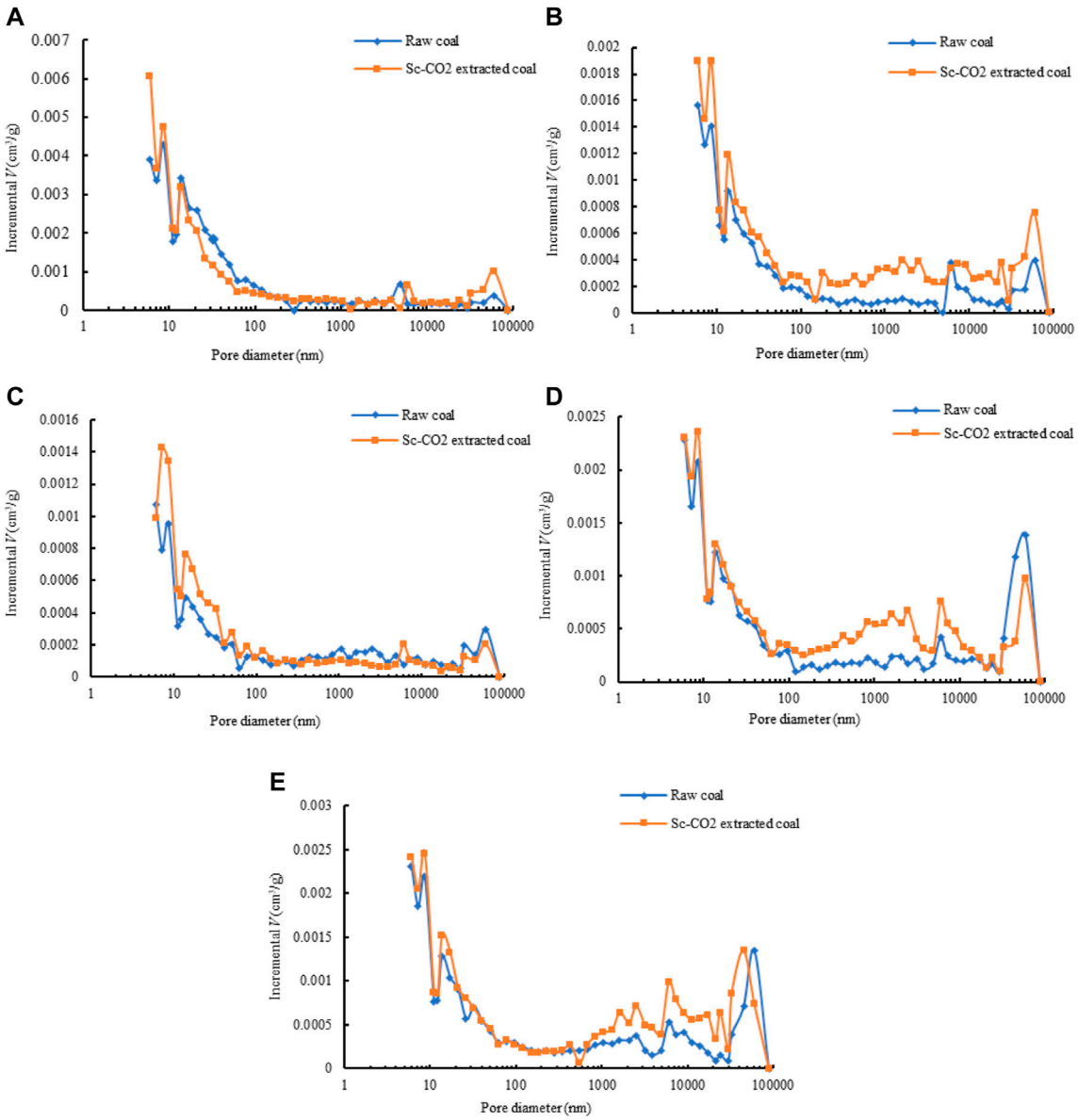

FIGURE 3
Pore volume distribution of the coal samples before and after Sc-CO_2 extraction **(A)** SJG coal; **(B)** LJZ coal; **(C)** LL coal; **(D)** CJW coal; and **(E)** SSP coal.

3.1 Pore structure change and its evolution

3.1.1 Pore volume change and its evolution

Table 2 presents the mercury injection pore volume test results of coal samples before and after Sc-CO_2 extraction, and the pore volume distributions of raw and Sc-CO_2 extracted coal are shown in Figure 3. The total pore volume of coal samples increased to different degrees after Sc-CO_2 extraction, and it was most significant for LJZ coal and SSP coal (Table 2). The pore volume of micropores and macropores increased more obviously after the Sc-CO_2 extraction of coal samples, and the increase of transitional pores and mesopores was smaller (Figure 3). After Sc-CO_2 extraction, the proportion of micropore and transitional pore volume decreased and that of the mesopore and macropore volume increased (Table 2).

In summary, the changes in pore volume and proportion of coal samples indicate that Sc-CO_2 extraction can increase the pore volume of coal, which is achieved by the increase in the number of pores and expansion of the pore diameter.

To determine the changes in pore volumes due to Sc-CO_2 extraction, ΔV can be defined by using the following equation:

$$\Delta V = V_B - V_A \tag{2}$$

where ΔV is the pore volume change due to Sc-CO_2 extraction, $cm^3 \cdot g^{-1}$; V_B is the pore volume of the sample after the Sc-CO_2 extraction, $cm^3 \cdot g^{-1}$; and V_A is the pore volume of the sample before the Sc-CO_2 extraction, $cm^3 \cdot g^{-1}$.

Figure 4 shows that the ΔV_{mi} and ΔV_{me} of coal are positive, and most of ΔV_{tr} and ΔV_{ma} are positive, indicating that Sc-CO_2 extraction causes the incremental pore volume to increase, and the incremental macropore volume makes up most of the total

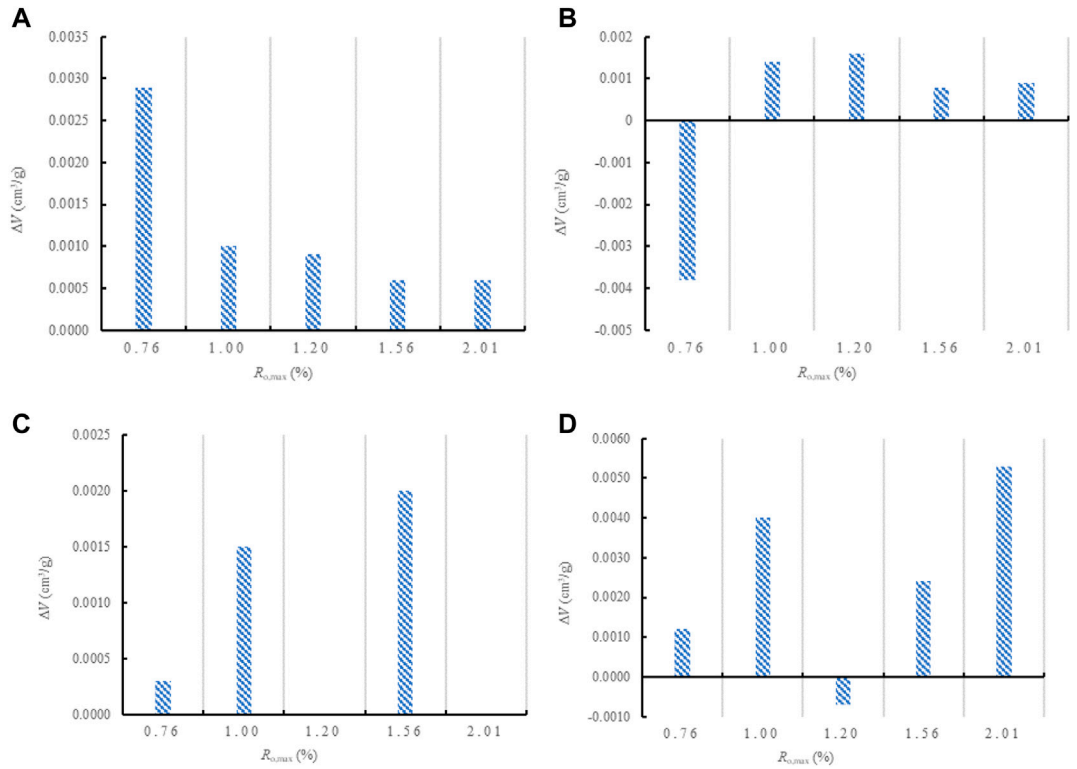

FIGURE 4
The changes in incremental pore volume of coal samples due to Sc-CO_2 extraction **(A)** Micropore; **(B)** Transitional pore; **(C)** Mesopore; and **(D)** Macropore.

TABLE 3 Pore-specific surface area of the samples before and after the Sc-CO_2 extraction.

Coal sample		Pore specific surface area ($m_2 \cdot g^{-1}$)					Proportion (%)			
		S_{mi}	S_{tr}	S_{me}	S_{ma}	S_t	S_{mi}/S_t	S_{tr}/S_t	S_{me}/S_t	S_{ma}/S_t
SJG	Raw coal	5.7888	3.8959	0.0432	0.0037	9.7316	59.49	40.03	0.44	0.04
	Sc-CO_2 extracted coal	6.2344	3.5285	0.0434	0.0032	9.8096	63.55	35.97	0.44	0.03
LJZ	Raw coal	2.1526	1.0716	0.0133	0.0017	3.2393	66.45	33.08	0.41	0.05
	Sc-CO_2 extracted coal	2.6499	1.3157	0.0297	0.0056	4.0008	66.23	32.88	0.74	0.14
LL	Raw coal	1.4347	0.6070	0.0129	0.0024	2.0570	69.75	29.51	0.63	0.12
	Sc-CO_2 extracted coal	1.8576	0.9348	0.0150	0.0015	2.8090	66.13	33.28	0.53	0.05
CJW	Raw coal	3.0500	1.4270	0.0200	0.0037	4.5007	67.77	31.71	0.44	0.08
	Sc-CO_2 extracted coal	3.3230	1.5519	0.0432	0.0089	4.9270	67.45	31.50	0.88	0.18
SSP	Raw coal	3.2190	1.4797	0.0286	0.0052	4.7325	68.02	31.27	0.60	0.11
	Sc-CO_2 extracted coal	3.4879	1.6981	0.0274	0.0097	5.2232	66.78	32.51	0.53	0.19

S_{mi}: Micropore specific surface area; S_{tr}: Transitional pore specific surface area; S_{me}: Mesopore specific surface area; S_{ma}: Macropore specific surface area; S_t: Total specific surface area.

pore volume. The relationship between incremental pore volume and coal rank was analyzed, and it was found that Sc-CO_2 extraction caused incremental pore volume to show an increasing–decreasing–increasing pattern with the increase of coal rank. The turning point is near the second coalification. Before the turning point, the incremental pore volume increases and then decreases with coal rank. After the turning point, the incremental pore volume increases gradually with coal rank. It is most significant in macropores.

3.1.2 Pore-specific surface area change and its evolution

Table 3 presents the mercury injection test results of the specific surface area of pores of coal samples before and after Sc-CO_2

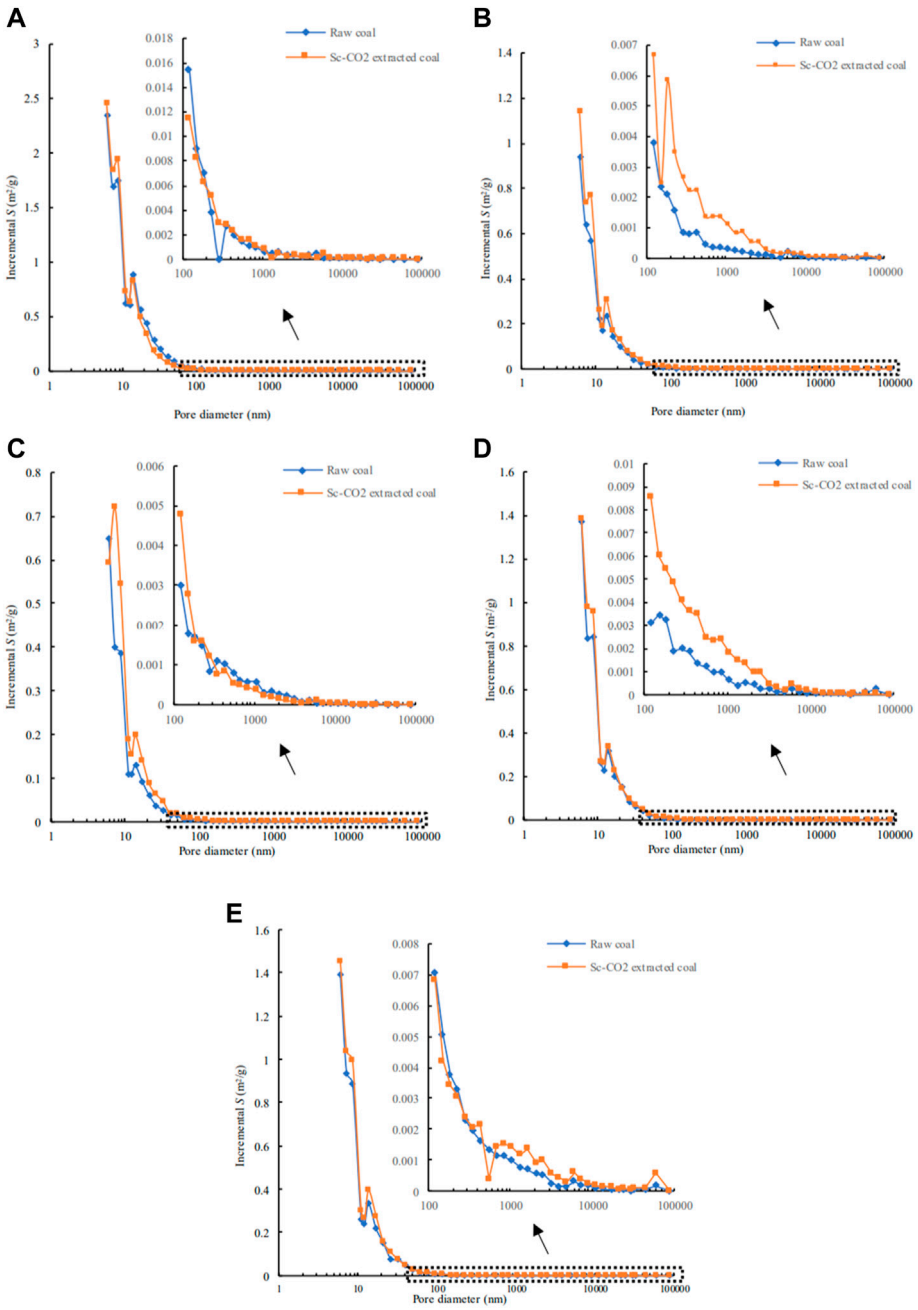

FIGURE 5
Pore-specific surface area distribution of the coal samples before and after Sc-CO_2 extraction **(A)** SJG coal; **(B)** LJZ coal; **(C)** LL coal; **(D)** CJW coal; and **(E)** SSP coal.

extraction, and the pore-specific surface area distributions of raw and Sc-CO_2 extracted coal are shown in Figure 5. The total specific surface area of pores of coal samples increased to different degrees after Sc-CO_2 extraction, and it was the most significant for LJZ coal and LL coal (Table 3). The specific surface area of micropores and transitional pores increased more obviously after the Sc-CO_2 extraction of coal samples, and the increase of mesopores and macropores was smaller (Figure 5). After Sc-CO_2 extraction, the proportion of micropores and transitional pore-specific surface area decreased, and a tendency was observed for the increase in the pore-specific surface area of mesopores and macropores (Table 3).

To determine the changes in pore-specific surface area due to Sc-CO_2 extraction, ΔS can be defined by using the following equation:

$$\Delta S = S_B - S_A \tag{3}$$

where ΔS is the pore-specific surface area change due to Sc-CO_2 extraction, $m_2 \cdot g^{-1}$; S_B is the pore-specific surface area of the coal sample after the Sc-CO_2 extraction, $m_2 \cdot g^{-1}$; and S_A is the pore-specific surface area of the coal sample before the Sc-CO_2 extraction, $m^2 \cdot g^{-1}$.

Figure 6 shows that the ΔS_{mi} values of coal are positive, and most of ΔS_{tr}, ΔS_{me}, and ΔS_{ma} are positive, indicating that the Sc-CO_2

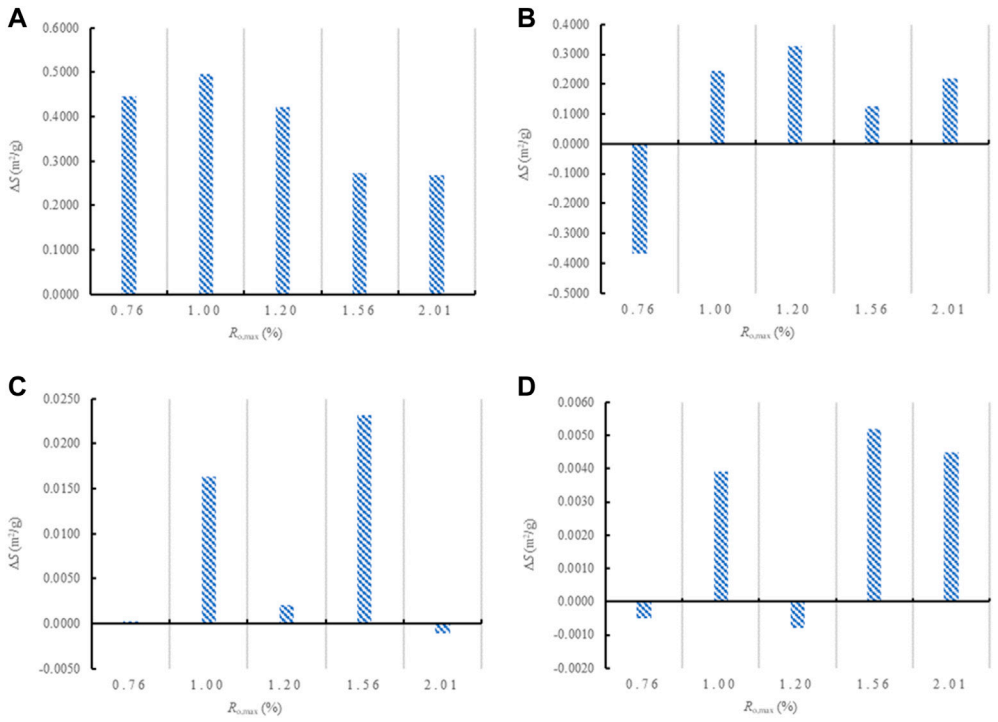

FIGURE 6
The changes of incremental pore-specific surface area of coal due to Sc-CO_2 extraction **(A)** Micropore; **(B)** Transitional pore; **(C)** Mesopore; and **(D)** Macropore.

extraction causes the incremental pore-specific surface area to increase and that the incremental micropore-specific surface area is the main contributor to the total pore-specific surface area. The relationship between incremental pore-specific surface area and coal rank was analyzed, and the results indicate that Sc-CO_2 extraction caused incremental pore-specific surface area to show an increasing–decreasing–increasing pattern with the increase of coal rank. The turning point was near the second coalification. Before the turning point, the incremental pore-specific surface area increased and then decreased with coal rank. After the turning point, the incremental pore-specific surface area increased gradually with coal rank. It is the most significant in transitional pores.

In summary, Sc-CO_2 extraction can not only increase the number of pores but also expand the pore volume. The analysis indicates that the main reason for this change is the precipitation of small organic molecules out of the coal by Sc-CO_2 extraction (Chen et al., 2017; Liu et al., 2018), which increases the number of open pores and also opens partially closed pores, acting as a pore increasing/expanding effect. Moreover, the evolution of pore volume and specific surface area increment with coal rank indicates that the pore volume and specific surface area of coal samples before and after Sc-CO_2 extraction change significantly near the second coalification. It indicates that the changes in pore structure during Sc-CO_2 extraction are controlled by coalification.

3.1.3 Pore morphology and its connectivity

Based on the experimental measurement data of mercury injection porosimetry, the mercury injection and ejection curves of coal samples were obtained (Figure 7). The volume of mercury withdrawn from the pores is less than the volume of mercury entering the pores at the same pressure; therefore, the mercury entering the coal pores cannot be completely discharged, which forms a hysteresis (Wu et al., 1991; Li and Zhou, 2021; Qi et al., 2022).

Figure 7 demonstrates that the maximum mercury injection of SJG coal slightly increased after Sc-CO_2 extraction, and the maximum mercury injection of LJZ, LL, CJW, and SSP coals significantly increased. The difference in the volume of mercury injection and ejection from coal samples before and after Sc-CO_2 extraction reveals that: (1) when small organic molecules present in open pores or pore throats are extracted and dissolved, the pores in coal get enlarged and pore throats are opened, resulting in the migration of mercury in the coal. (2) When small organic molecules present in closed pores or ink bottle pores in coal are partially precipitated after Sc-CO_2 extraction, some pores can be opened or converted into new ink bottle-shaped pores. With the conversion of the sealed pores into new ink bottle-shaped pores, mercury trapped in coal increases.

Sc-CO_2 extraction dissolves small organic molecules present in coal, making the closed and semi-closed pores in coal transit to open pores, and some micron-sized pores are opened, which plays a role in increasing coal pores and improving porosity.

3.2 Porosity change and its evolution

The results of the transverse relaxation time T_2 spectrum of the coal samples before and after Sc-CO_2 extraction are shown in Figure 8. The amplitude and area of the T_2 spectrum of coal samples increased gradually after Sc-CO_2 extraction, indicating that Sc-CO_2 extraction

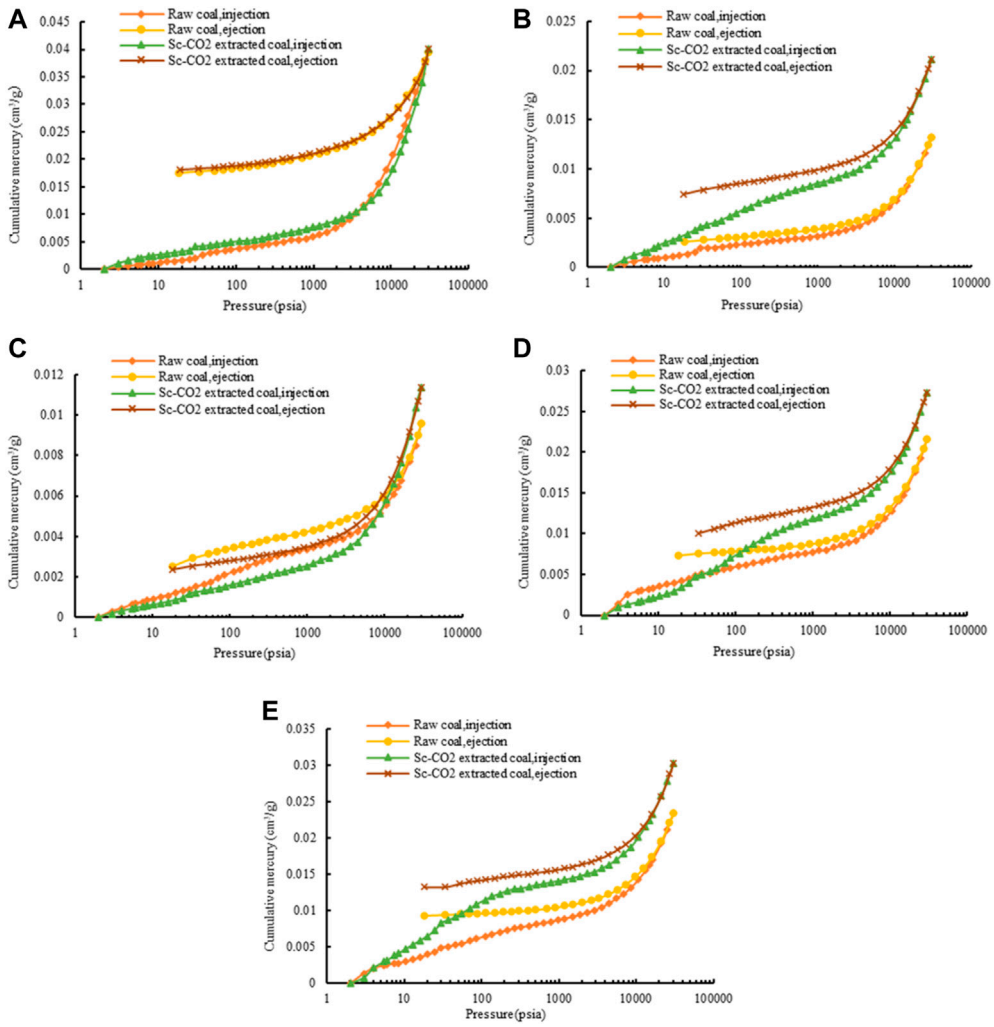

FIGURE 7
Mercury injection and ejection of coal samples **(A)** SJG coal; **(B)** LJZ coal **(C)** LL coal; **(D)** CJW coal; and **(E)** SSP coal.

could transform the pore structure of coal and promote the development of pores.

Based on the NMR spectroscopy principle, the T_2 peaks corresponding to each pore segment were identified by the NMR test results. The T_2 peaks corresponding to microporous and transitional pores are located in the range of 0.1–0.15 m, those corresponding to mesopores are present in the range of 5–55 m, and the T_2 peaks corresponding to large pores are located in the segment greater than 80 m.

The porosity of the coal sample can be obtained by using the T_2 spectrum of coal samples obtained under saturated water conditions. The specific implementation methods are as follows: (1) Measurement of the porosity of a certain volume of known samples, and establishment of a relationship equation between the NMR unit volume signal and porosity, as shown in Figure 9; (2) The test coal samples are measured by NMR spectroscopy, and the NMR unit signal of coal samples under saturated water and bound water conditions is substituted into the relationship equation with porosity (see equation in Figure 9) for calculation.

Table 4 lists the porosity test results of the coal sample before and after Sc-CO_2. The total porosity of coal samples increased to different degrees after Sc-CO_2 extraction, and it was the most significant for SSP coal. The porosity of micropore and macropore increased significantly, and that of transitional pore and mesopore increased or decreased. After Sc-CO_2 extraction, the proportion of micropore and transitional pore porosity decreased, while the proportion of mesopore and macropore porosity increased.

To determine the changes in porosity due to Sc-CO_2 extraction, ΔP can be defined by using the following equation:

$$\Delta P = P_B - P_A \tag{4}$$

where ΔP is the porosity change due to Sc-CO_2 extraction, %; P_B is the porosity of the coal sample after the Sc-CO_2 extraction, %; and P_A is the porosity of the coal sample before the Sc-CO_2 extraction, %.

Figure 10 exhibits that the ΔP_{ma} values of coal are positive, and most of ΔP_{mi}, ΔP_{tr}, and ΔP_{me} are positive, indicating that the Sc-CO_2 extraction leads to an increase in incremental porosity, and incremental macropore porosity is the main contributor to total porosity. The relationship between incremental porosity and coal rank was analyzed, and it was found that Sc-CO_2 extraction caused

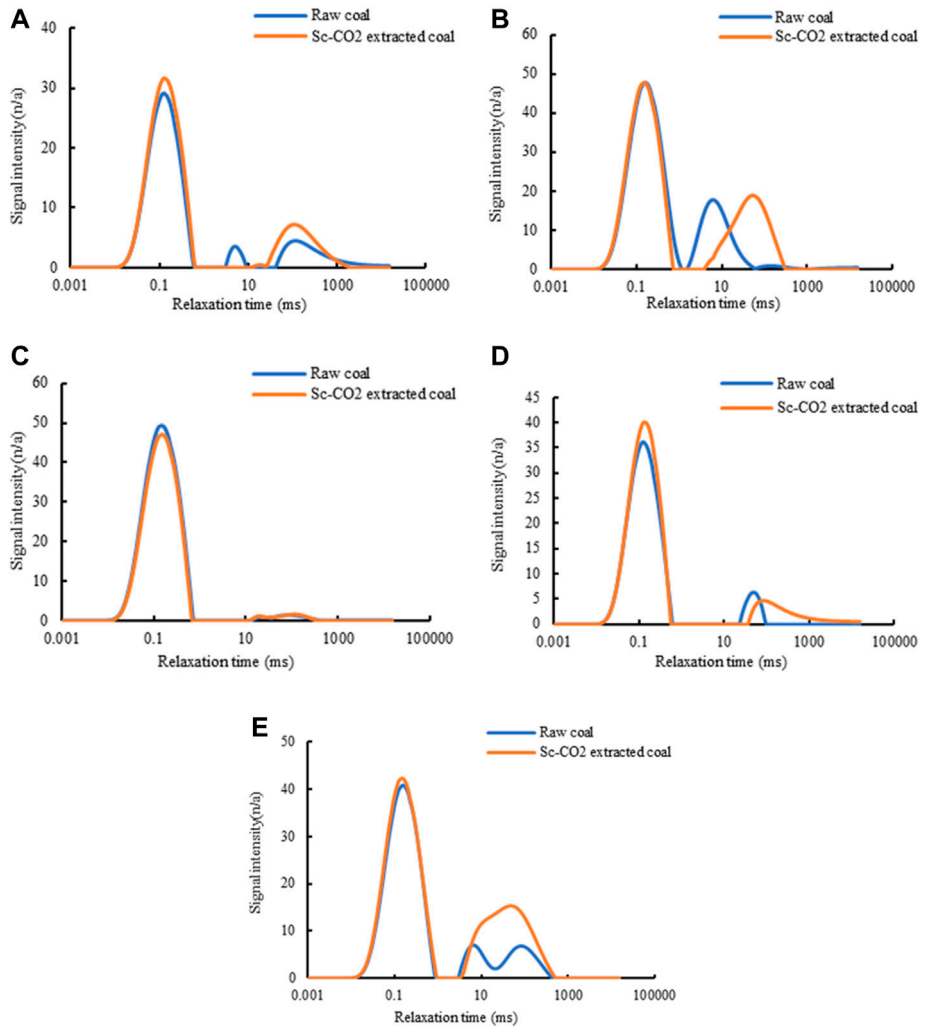

FIGURE 8
Transverse relaxation time T_2 spectrum of coal sample **(A)** SJG coal; **(B)** LJZ coal; **(C)** LL coal; **(D)** CJW coal; and **(E)** SSP coal.

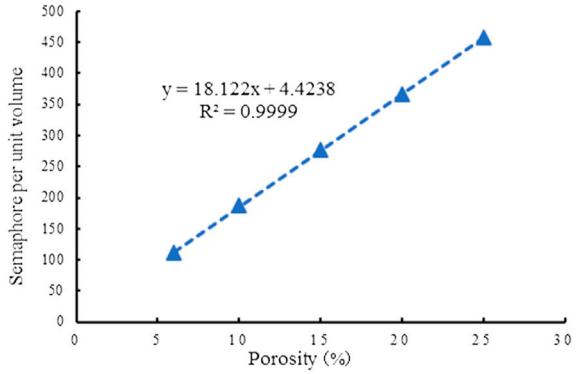

FIGURE 9
Calibration curve.

incremental porosity to present an increasing–decreasing–increasing trend with the increase of coal rank. The turning point was near the second coalification. Before the turning point, incremental porosity increases and then decreases with coal rank. After the turning point, incremental porosity increases gradually with coal rank. It is the most significant in micropore and mesopore porosity.

In summary, the variation of porosity increment with coal rank under Sc-CO_2 extraction is similar to that of pore volume and pore-specific surface area. The results of the NMR test and mercury intrusion porosimetry test are mutually corroborated, which proves again that Sc-CO_2 extraction exhibits an obvious transformation effect on pore structure in coal.

3.3 Pore structure evolution model

According to the previous discussion, Sc-CO_2 extraction exhibits a dual effect of increasing and expanding pores on the transformation of the pore structure of coal. The increasing pore effect mainly occurs in the micropores, and the expanding pore effect mainly occurs in the transitional pores and the above-mentioned pores. The change of pore structure of coal by Sc-CO_2 extraction is controlled by coalification.

TABLE 4 The porosity of coal samples before and after Sc-CO_2 extraction.

Coal sample		Porosity (%)					Proportion (%)			
		P_{mi}	P_{tr}	P_{mc}	P_{ma}	P_t	P_{mi}/P_t	P_{tr}/P_t	P_{mc}/P_t	P_{ma}/P_t
SJG	Raw coal	0.8256	0.0074	0.0415	0.0283	0.9028	91.45	0.82	4.60	3.13
	Sc-CO_2 extracted coal	0.7832	0.0031	0.0071	0.1125	0.9059	86.46	0.34	0.78	12.42
LJZ	Raw coal	0.7371	0.0203	0.0203	0.1397	0.9174	80.35	2.21	2.21	15.23
	Sc-CO_2 extracted coal	1.0529	0.0148	0.0346	0.2465	1.3488	78.06	1.10	2.57	18.28
LL	Raw coal	1.0864	0.0348	0.0109	0.0248	1.1569	93.91	3.01	0.94	2.14
	Sc-CO_2 extracted coal	1.1070	0.0266	0.0167	0.0289	1.1792	93.88	2.26	1.42	2.45
CJW	Raw coal	1.6223	0.3052	0.3717	0.0437	2.3429	69.24	13.03	15.86	1.87
	Sc-CO_2 extracted coal	1.6859	0.0594	0.4425	0.3546	2.5424	66.31	2.34	17.40	13.95
SSP	Raw coal	1.1298	0.0882	0.1376	0.1317	1.4873	75.96	5.93	9.25	8.85
	Sc-CO_2 extracted coal	1.4258	0.1051	0.4751	0.3256	2.3316	61.15	4.51	20.38	13.96

P_{mi}: Micropore porosity; P_{tr}: Transitional porosity; P_{mc}: Mesopore porosity; P_{ma}: Macropore porosity; P_t: Total porosity.

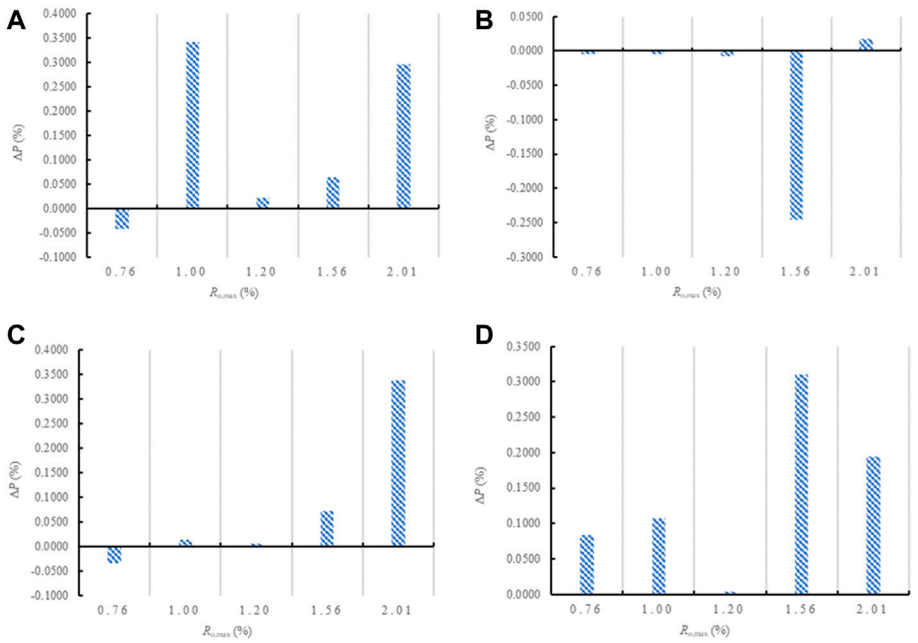

FIGURE 10
The changes in incremental porosity of coal due to Sc-CO_2 extraction **(A)** Micropore; **(B)** Transitional pore; **(C)** Mesopore; and **(D)** Macropore.

The mechanisms of Sc-CO_2 extraction affecting coal pore structure are attributed to the dissolution of small organic molecules in Sc-CO_2 fluid. In order to describe the pore structure evolution characteristics of coal based on Sc-CO_2 extraction, according to the related previous research results (Chen et al., 2017; Su et al., 2018; Wang et al., 2022) and the analysis of results of this study, the evolution model of pore structure of coal by Sc-CO_2 extraction was established (Figure 11). In the process of coalification, under the influence of coalification, temperature, and pressure, the branches and side chains in the macromolecular structure of organic matter present in coal continuously fall off to form small organic molecules in coal, which get filled in the pore structure of coal to form closed or semi-closed organic filling pores (Figure 11A). After Sc-CO_2 extraction, the small organic molecules present in the pore structure of filled coal are partially extracted, resulting in the increase of pore volume, specific surface area, and porosity of coal to varying degrees. Owing to the short extraction time, some organic small molecules still do not get extracted completely (Figure 11B). At the same time, the pore throats originally filled with small organic molecules (Figure 11C) are likely to be opened from open pores (Figure 11D) after Sc-CO_2 extraction, and the porosity of coal pores becomes better.

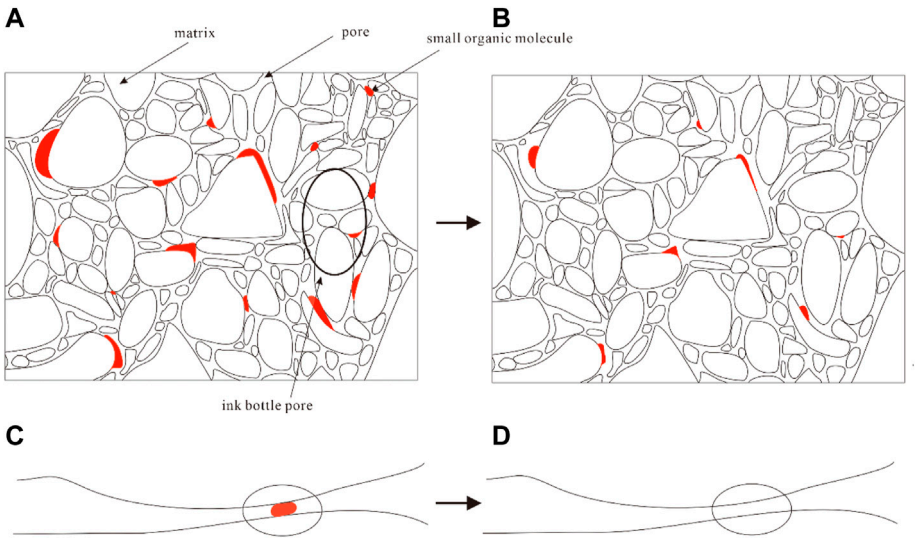

FIGURE 11
Hypothetical model of sample pore structure evolution **(A)** Pore structure of raw coal; **(B)** Pore structure of Sc-CO_2 extraction coal **(C)** Raw coal throat; **(D)** and Sc-CO_2 extraction coal throat.

4 Conclusion

The Sc-CO_2 extraction device was used to simulate the extraction process of CO_2-ECBM under geological conditions, and the mercury intrusion porosimetry and NMR spectroscopy tests were conducted to test the pore structure and porosity of coal before and after CO_2 extraction. Based on the results, the following conclusions can be drawn.

1) Pore volume, pore-specific surface area, and connectivity characteristics changed significantly by Sc-CO_2 extraction, and the increment of pore volume and pore-specific surface area presented an increasing–decreasing–increasing trend with the increase in the coal rank, and the turning point was found to be near the second coalification.
2) The porosity change due to Sc-CO_2 extraction increased–decreased–increased with increasing coal rank, the turning point was also near the second coalification, which supports the mercury intrusion porosimetry results.
3) The changes were observed in the porosity characteristics due to Sc-CO_2 extraction through pore-increasing and expanding effects. Before the second coalification, the pore-increasing and expanding effects co-existed in the micropores; however, after the second coalification, the pore-expanding effect mainly existed in transitional pores and above.
4) Based on the research, the pore structure evolution model of Sc-CO_2 extraction of coal was established.
5) The extraction time of this study was short, which may be different from the effect of Sc-CO_2 extraction on coal pores under geological conditions. Undeniably, a lot more systematic explorations are further demanded to investigate the time effect of Sc-CO_2 extraction on coal pore characteristics, which will be pursued in the future.

Data availability statement

The raw data supporting the conclusions of this article will be made available by the authors, without undue reservation.

Author contributions

RC designed the facilities and experiments; RC, KH, and FL performed the experiment and analyzed the data; RC, KH, and YZ compiled the data and plotted the graphs; RC wrote the paper.

Funding

This research was funded by the Fundamental Research Funds for the Central Universities (2019XKQYMS24). The authors express their appreciation to by the Fundamental Research Funds for the Central Universities (2019XKQYMS24) for the financial support of this work. Experiments were conducted at China University of Mining and Technology.

Acknowledgments

We would like to thank a number of research students from China University of Ming and Technology for their assistance in the coal sampling and some experiments.

Conflict of interest

The authors declare that the research was conducted in the absence of any commercial or financial relationships that could be construed as a potential conflict of interest.

Publisher's note

References

Chen, R., Qin, Y., Wei, C. T., Wang, L. L., Wang, Y. Y., and Zhang, P. F. (2017). Changes in pore structure of coal associated with Sc-CO_2 extraction during CO_2-ECBM. *Appl. Sci.* 7, 931. doi:10.3390/app7090931

Chen, Y. P., Jiang, W. Z., Qin, Y. J., and Su, W. W. (2021). Review on research theory and methods of pore distribution characteristics of coal. *Saf. Coal Mines* 52, 190–196. doi:10.13347/j.cnki.mkaq.2021.03.035

Di, G., Guo, H. L., Guo, B. Q., Kaili, T., and Ren, H. X. (2022). Impact of microbially enhanced coalbed methane on the pore structure of coal. *Front. Earth Sci.* 10. doi:10.3389/feart.2022.869917

Du, Y., Sang, S. X., Wang, W. F., Liu, S. Q., Wang, T., and Fang, H. H. (2018). Experimental study of the reactionsa of supercritiacal CO_2 and minerals in high-rank under formation conditions. *Energy Fuels* 32, 1115–1125. doi:10.1021/acs.energyfuels.7b02650

Fu, X. H., Qin, Y., Zhang, W. H., Wei, C. T., and Zhou, R. F. (2005). Study on fractal classification and natural classification of coal pores based on coalbed methane transport. *Sci. Bull.* 50, 51–55. doi:10.3321/j.issn:0023-074X.2005.z1.009

Fu, X. H., Qin, Y., and Wei, C. T. (2007). *Coal bed methane geology*. Xuzhou: China university of mining and technology press.

Guo, H., Ni, X. M., Wang, Y. B., Du, X. M., Yu, T. T., and Feng, R. M. (2018). Expeimental study of CO_2-water-mineral interactions and their influence on the permeability of coking coal and implications for CO_2-ECBM. *Minerals* 8, 117. doi:10.3390/min8030117

Li, J. R., and Zhou, Q. Z. (2021). "Characterization of the pore structure of coal samples based on mercury-pressure experiments," in Proceedings of the 27th annual academic conference of the Beijing Mechanics Society, 1299–1302. doi:10.26914/c.cnkihy.2021.001964

Liu, S. Q., Ma, J. S., Sang, S. X., Wang, T., Du, Y., and Fang, H. H. (2018). The effects of supercritical CO_2 on mesopore and macropore structure in bituminous and anthracite coal. *Fuel* 233, 32–43. doi:10.1016/j.fuel.2018.03.036

Liu, J., Xie, L. Z., Elsworth, D., and Gan, Q. (2019). CO_2/CH_4 competitive adsorption in shale: Implications for enhancement in gas production and reduction in carbon emissions. *Environ. Sci. Technol.* 15, 9328–9336. doi:10.1021/acs.est.9b02432

Liu, H. F., Song, D. Z., He, X. Q., Tian, X. H., Lou, Q., and Wang, W. X. (2020). Influence of coalification on microstructure characteristics of coal surface. *China Saf. Sci. J.* 30, 121–127. doi:10.16265/j.cnki.issn1003-3033.2020.01.019

Liu, Y. W., Zhang, X. M., and Miao, J. (2020). Study on evolution of pore structure of medium and high rank coals. *Saf. Coal Mines* 51, 7–13. doi:10.13347/j.cnki.mkaq.2020.11.003

Liu, H. Q., Wang, L., Xie, G. X., Yuan, Q. P., Zhu, C. Q., and Jiao, Z. H. (2022). Comprehensive characterization anf full pore size fractal characteristics of coal pore structure. *J. Min. Saf. Eng.* 39, 458–469. doi:10.13545/j.cnki.jmse.2021.0630

Lv, Z. F., Zhang, X. M., Zhong, L. W., Zhang, S. A., Zhu, Z. Y., and Li, J. (1991). Pore characteristics of lump coal and its influencing factors. *J. China Univ. Ming Technol.* 20, 48–57.

Qi, L. L., Zhou, X. Q., Peng, X. S., Wang, Z. F., and Dai, J. H. (2022). Study on pore structure of coking coal based on low-temperature nitrogen adsorption and mercury intrusion method. *Saf. Coal Mines* 53, 1–6. doi:10.13347/j.cnki.mkaq.2022.07.002

Sampath, K. H. S. M., Sin, I., Perera, M. S. A., Matthai, S. K., Ranjith, P. G., and Li, D. Y. (2020). Effect of supercritical CO_2 interaction time on the alterations in coal pore structure. *J. Nat. Gas Sci. Eng.* 76, 103214. doi:10.1016/j.jngse.2020.103214

Si, L. L., Ping, J., Xi, Y. J., Wang, H. Y., Wen, Z. H., Li, B., et al. (2021). The influence of long-time water intrusion on the mineral and pore structure of coal. *Fuel* 290, 119848. doi:10.1016/J.fuel.2020.119848

Su, E. L., Liang, Y. P., Li, L., Zou, Q. L., and Niu, F. F. (2018). Laboratory study on changes in the pore structures and gas desorption properties of intact and tectonic coals after supercritical CO_2 treatment: Implications for coalbed methane recovery. *Energies* 11, 3419. doi:10.3390/en11123419

Tang, S. H., Cai, C., Zhu, B. C., Duan, L. J., and Zhang, J. Z. (2008). The control of the degree of coal metamorphism on the physical properties of coal reservoirs. *Nat. Gas. Ind.* 28, 30–33. doi:10.3787/j.issn.1000-0976.2008.12.007

Wang, S. W., and Chen, Z. H. (1995). Progress in the study of pore and fracture systems in coal reservoirs. *Geol. Sci. Technol. Inf.* 14, 53–59.

Wang, Z. Z., Pan, J. N., Hou, Q. L., Yu, B. S., Li, M., and Niu, Q. H. (2018). Anisotropic characteristics of low-rank coal fractures in the Fukang mining area, China. *Fuel* 211, 182–193. doi:10.1016/j.fuel.2017.09.067

Wang, Z. Z., Fu, X. H., Hao, M., Li, G. F., Pan, J. N., Niu, Q. H., et al. (2021). Experimental insights into the adsorption-desorption of CH_4/N_2 and induced strain for medium-rank coals. *J. Petroleum Sci. Eng.* 204, 108705. doi:10.1016/J.petrol.2021.108705

Wang, X. L., Geng, J. B., Zhang, D. M., Xiao, W. J., Chen, Y., and Zhang, H. (2022). Influence of sub-supercritical CO_2 on pore structure and fractal characteristics of anthracite: An experimental study. *Energy* 261, 125115. doi:10.1016/J.energy.2022.125115

Wang, Y. Y. (2018). *Supercritical CO_2 extraction coal adsorption characteristics and its mechanism*. China: China University of Mining and Technology.

Washburn, E. W. (1921). The dynamics of capillary flow. *Am. Phys. Soc.* 17, 273–283. doi:10.1103/physrev.17.273

Wu, J., Jin, K. L., Tong, Y. D., and Qian, R. D. (1991). Coal pore theory and its application in gas protrusion and extraction evaluation. *J. China Coal Soc.* 86, 95.

Wu, S., Tang, D. Z., Xu, H., and Li, S. (2016). Characeristics of pore development in medium-high rank coal. *Coal Geol. Explor.* 44, 69–74. doi:10.3969/j.issn.1001-1986.2016.06.013

Xiong, J. L., Wang, K., Du, Q. X., Meng, X. C., and Guo, B. B. (2022). Study on pore characteristics of acidified coal samples based on low field nuclear magnetic resonance technology. *Min. Saf. Environ. Prot.* 49, 47–52. doi:10.19835/j.issn.1008-4495.2022.01.008

Xu, H. G., and Qin, X. G. (2022). Study on the influence of cooking coal pore structure on meathane desorption in Xishan coalfield. *Saf. Coal Mines* 53, 7–12. doi:10.13347/j.cnki.mkaq.2022.05.002

Yang, M., Liu, L., Zhang, X. B., Mao, J. R., and Cai, P. (2021). Nucler magnetic resonance experimental study on pore structure and fluid characteristics of coal at different ranks. *China Saf. Sci. J.* 31, 81–88. doi:10.16265/j.cnki.issn1003-3033.2021.01.012

Yuan, J. W., Xia, J. Y., Wang, Y., Chen, M., and Chen, J. X. (2022). Effect of freeze-thaw cycles on coal pore structure and gas emission characteristics. *Acs Omega* 7, 16087–16096. doi:10.1021/acsomega.2C01413

Zhang, K., Sang, S. X., Liu, C. J., Ma, M. Y., and Zhou, X. Z. (2019). Experimental study the influences of geochemical reaction on coal structure during the CO_2 geological storage in deep coal seam. *J. Petroleum Sci. Eng.* 178, 1006–1017. doi:10.1016/j.petrol.2019.03.082

Zhang, D. F., Li, C., Li, Y. H., and Jiang, W. P. (2020). Progress in the study of the relationship between CO_2 fluids and mineral interaction in coal during sequestration. *J. Saf. Environ.* 20, 297–309. doi:10.13637/j.issn.1009-6094.2019.0568

Zhang, H. (2001). Genesis types of coal pore space and its study. *J. China Coal Soc.* 26, 40–44. doi:10.3321/j.issn:0253-9993.2001.01.009

Zhang, P. F. (2019). *Study on the characteristics of pore permeation changes of supercritical CO_2 extracted coal*. China: China University of Mining and Technology.

Zhao, X. L., Tang, D. Z., Xu, H., Tao, S., and Chen, Z. L. (2010). Effect of coal matamorphic process on pore system of coal resevoirs. *J. China Coal Soc.* 35, 1506–1511. doi:10.13225/j.cnki.jccs.2010.09.009

Zhao, P., He, B., Zhang, B., and Liu, J. (2022). Porosity of gas shale: Is the NMR-based measurement reliable? *Petroleum Sci.* 19, 509–517. doi:10.1016/j.petsci.2021.12.013

Zheng, S. J., Yao, Y. B., Liu, D. M., Cai, Y. D., and Liu, Y. (2018). Characterizations of full-scale pore size distribution, porosity and permeability of coals: A novel methodology by nuclear magnetic resonance and fractal analysis theory. *Int. J. Coal Geol.* 196, 148–158. doi:10.1016/j.coal.2018.07.008

Zheng, S. J., Yao, Y. B., Liu, D. M., Cai, Y. D., Liu, Y., and Li, X. W. (2019). Nuclear magnetic resonance T_2 cutoffs of coals: A novel method by multifractal analysis theory. *Fuel* 241, 715–724. doi:10.1016/j.fuel.2018.12.044

Zhu, Q. Z., Yang, Y. H., Lu, X. Q., Liu, D. M., Li, X. W., Zhang, Q. Q., et al. (2019). Pore structure of coals by mercury intrusion, N_2 adsorption and NMR: A comparative study. *Appl. Sci.* 9, 1680. doi:10.3390/app9081680

Чодот, B. B. (1966). *Coal and gas outburst*. Beijing: China industry press. Wang Y A. translation.